combined approach may be taken into the future. The key to successful icing forecasting lies in understanding the physical processes resulting in supercooled liquid water production, how these processes relate to observable phenomena, and how to combine information from as many sources as possible to gain the most complete picture of the icing situation.

Glossary

Supercooled Refers to liquid water cooled to below 0°C without becoming a solid (ice).

Glaze ice Ice with a translucent, glossy appearance. May be smooth or have embedded lumps. Sometimes referred to as 'clear' ice.

Rime ice Opaque, brittle ice that tends to form 'feathers' into the airstream.

Mixed ice A combination of rime and glaze ice, caused by variations in atmospheric parameters resulting in either type of ice.

Severity Refers to the combination of environmental icing intensity, aircraft response, and pilot interpretation of that response.

See also

Cloud Microphysics. **Cyclones, Extra Tropical**. **Humidity Variables**. **Mesoscale Meteorology:** Overview. **Mountain Meteorology**. **Parameterization of Physical Processes:** Clouds. **Radar:** Precipitation Radar. **Satellite Remote Sensing:** Precipitation; Temperature Soundings; Water Vapor. **Thermodynamics:** Moist (Unsaturated) Air. **Weather Prediction:** Regional Prediction Models.

Further Reading

Cooper WA, Sand WR, Politovich MK and Veal DL (1984) Effects of icing on performance of a research airplane. *Journal of Aircraft* 21: 708–715.

Hansman RJ Jr (1985) Droplet size distribution effects on aircraft ice accretion. *Journal of Aircraft* 22: 503–508.

Lankford TT (2000) *Aircraft Icing: A Pilot's Guide* (Practical Flying Series). New York: McGraw-Hill.

Matrosov SY, Reinking RF, Kropfli RA and Bartram BW (1996) Estimation of ice hydrometeor types and shapes from radar polarization measurements. *Journal of Atmospheric and Oceanic Technology* 13: 85–96.

Politovich MK (1995) Response of a research aircraft to icing and evaluation of severity indices. *Journal of Aircraft* 33: 291–297.

Schultz P and Politovich MK (1991) Toward the improvement of aircraft icing forecasting for the continental United States. *Weather and Forecasting* 7: 491–500.

Thompson G, Bruintjes RT, Brown BG and Hage F (1997) Intercomparison of in-flight icing algorithms. Part I: WISP94 Real-time Icing Prediction and Evaluation Program. *Weather and Forecasting* 12: 878–889.

AIR–SEA INTERACTION

Contents

Freshwater Flux

J Schulz, Meteorological Institute, University of Bonn, Bonn, Germany

Introduction

The world ocean is a key element of the physical climate system. The ocean contains 97% of the world's water and covers an area of 71% of the globe. As a reservoir, the ocean supplies water vapor to the atmosphere that brings rain and snow over land surfaces. About one-third of the precipitation over

land originates from water evaporated from the ocean. The water vapor in the atmosphere is the most important gaseous absorber for solar and terrestrial radiation and accounts for about half of the atmosphere's natural greenhouse effect. The process of evaporation accounts for approximately half of the surface cooling balancing the heating by absorption of solar radiation.

Because of the asymmetric insolation of the Earth's surface by solar radiation, the oceans act as a large energy and heat transport system from the Equator to the poles. The deep-ocean circulation that is critical for this transport is mostly driven by variations in the density of sea water. Ocean salinity is an important contributor to these variations and varies with latitude in the upper layers of the oceans. The surface salinity depends on the fresh water flux at the ocean surface and is relatively high in the subtropics where evaporation exceeds precipitation, whereas it is relatively low in the tropics and middle and high latitudes where precipitation dominates.

The most comprehensive publication about the world water balance was written by Baumgartner and Reichel in 1975. They assembled different estimates of the water balance over continents, river basins, and oceans to calculate a global water balance. This pioneering work resulted in global maps of evaporation and precipitation that even today are widely used by meteorologists, oceanographers, climatologists, and hydrologists. The definition of the water balance and its components used here follows the work of Baumgartner and Reichel.

Assuming that the amount of water on Earth is not changing with time, the long-term average of the water balance for a unit area of the Earth's surface can be written as eqn [1].

$$P = E + D \qquad [1]$$

In eqn [1], P is precipitation, E is evaporation, and D is discharge or river runoff. This balance states that water added to the surface by precipitation is partitioned between E and D. Although globally precipitation and evaporation are balanced, the large differences in the components P, E, and D over land and over ocean produce the world's water cycle, shown schematically in **Figure 1**. The units used throughout the chapter for E, P, and $E-P$ are mm d^{-1}. In general, total evaporation exceeds precipitation over oceans, which is compensated for by the runoff of rivers from the continents, where precipitation exceeds evaporation.

In the following sections the focus will be on the different methods used to determine the freshwater flux at the oceans surface: E, P, $E-P$ will be considered in detail. The heat transport within the oceans is beyond the scope of this article (*see* **Air–Sea Interaction:** Momentum, Heat and Vapor Fluxes). The second section gives an overview of different techniques that can be used to determine the fresh water flux, followed by a description of the fresh water flux climatology as derived from satellite data. This is followed by a short consideration of the role of river runoff, and finally some conclusions are presented.

Methods for Determining *E*, *P*, and *E*–*P*

Basically, there exist three different methods for determining the components E and P as well as

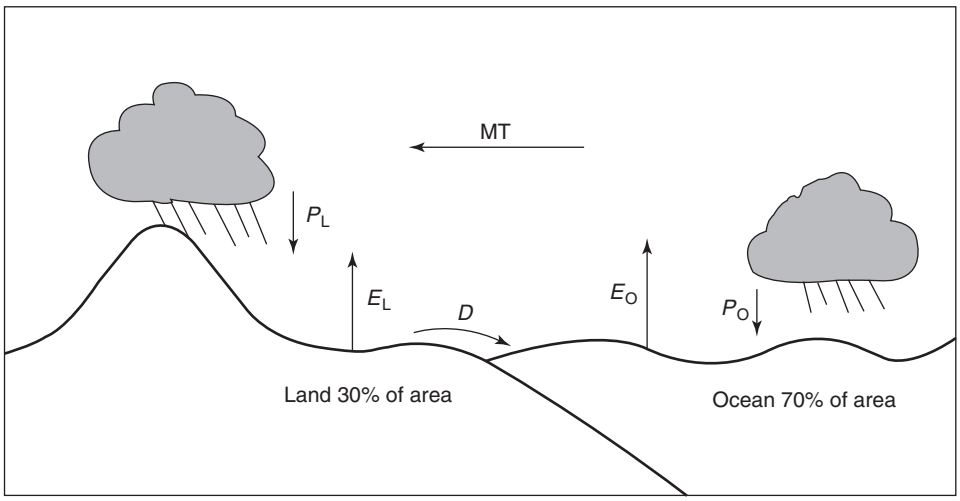

Figure 1 Schematic representation of the world water cycle E and P denote evaporation and precipitation over oceans and land (denoted by subscript O and L, respectively). D is the discharge or river runoff of water from the continents to the oceans and MT is the moisture transport in the atmosphere.

$E - P$. Traditional estimates of E are based on *in situ* measurements of surface wind speed U, specific humidity of air Q_a, and sea surface temperature T_S. These are used within the so-called bulk aerodynamic formula to parametrize the evaporation (*see* **Turbulent Diffusion**). P is estimated by analyzing actual weather reports using an empirical parametrization. The resulting estimates are interpolated and extrapolated to construct global maps of E and P.

Recently, satellite data have been used to derive the same basic state variables near and at the ocean surface using empirical and physical retrieval schemes. Again these quantities are used to parametrize E using the bulk aerodynamic formula. Many algorithms for estimating rainfall using almost the whole electromagnetic spectrum have been developed during the last 20 years (*see* **Satellite Remote Sensing:** Precipitation). These satellite algorithms are used alone and in conjunction with *in situ* data and model results to give best estimates.

The third method is the so-called moisture budget method, which make use of global-scale analyzed water vapor fields or measurements of atmospheric water vapor by rawinsondes in the form of four-dimensional data assimilation (*see* **Data Analysis:** Time Series Analysis). The global distribution of $E - P$ is then computed from the residuals of water vapor transport in the atmosphere using large-scale numerical models.

Traditional Estimates from *in situ* Measurements

Most of our present knowledge of fresh water fluxes is derived from weather observations on special weather ships, buoy data, and also data from merchant ships participating in the Voluntary Observing Ship system. Many of these data have been organized into the Comprehensive Ocean Atmosphere Data Set which has been used to derive climatologies of the energy fluxes and the fresh water flux at the sea surface. The major disadvantage of ship-based estimates of E and P is that the observation base is not very good for either parameter. The coverage is mostly obtained along shipping lanes, which may be sufficient in the North Atlantic, North Pacific, and the Mediterranean but is not sufficient in the Tropics and all southern oceans. Additionally, the concentration along shipping lanes can introduce a fair weather bias, since ships try to avoid bad weather.

Whereas the measurement quality for the basic state variables used for the parametrization of E is relatively good on ocean weather ships and research quality buoys, it is less good on the voluntary observing ships. Although much effort has been put into correcting errors on the basis of individual ship measurements during the last few years, the global heat balance has not been closed, mostly because of the low observation density and deficiencies in the bulk aerodynamic formula. The determination of precipitation is even more difficult. It is largely based on the observed actual weather and parametrizations that convert the weather code into rainfall amount. The conversion schemes were developed from data that are not representative of the global oceans, so it became necessary to correct under-estimated precipitation in the Tropics by empirical temperature-dependent corrections. Incorporation of P measurements from islands in data-sparse regions is also very difficult, because of the influence of island terrain on the rainfall. Comparisons of these precipitation fields with satellite-derived fields exhibit large differences even at the climatological scale.

Remote Sensing of $E - P$

Remote sensing of evaporation is based mostly upon the derivation of basic state variables, wind speed, sea surface temperature, and near-surface atmospheric specific humidity, and the parametrization of the evaporation using the bulk aerodynamic formula. Wind speed can be obtained from either passive or active microwave systems. The active system relates the backscattered energy to the wind speed at a reference level over sea surface (e.g., 10 m) and is also able to deliver wind direction information. The passive systems rely on the surface emission change due to wind-induced sea surface roughness and partial foam coverage. The root-mean-square (rms) errors on an instantaneous time scale for both systems are on the order ± 1.3 to $\pm 2\,\mathrm{m\,s^{-1}}$. Remote sensing methods for the near-surface specific humidity make use of a vertically integrated water vapor content (obtained from a passive microwave instrument such as the Special Sensor Microwave/Imager (SSM/I)) as a predictor. Several techniques ranging from linear regression analysis to neural networks have been used to deduce the near-surface humidity with rms errors of $\sim \pm 0.7\,\mathrm{g\,kg^{-1}}$ on the monthly time scale. Estimates of sea surface temperature are deduced from passive infrared sensors like the Advanced Very High Resolution Radiometer (AVHRR). The largest problem with this method is the cloud clearance of the satellite scene, because otherwise the determined T_S would be negatively biased. Accounting for the surface skin effect, rms errors for the best satellite methods are $\sim \pm 0.2$ K. Estimates of sea surface temperature with not much less accuracy are also possible employing passive microwave measurements at frequencies between $\sim$5–10 GHz that are available from TRMM's TMI and will shortly be available from the new Advance Multifrequency Scanning Radiometer onboard the

Aqua and ADEOS-II satellites. The big advantage of those estimates is the much better coverage because clouds are almost transparent at those frequencies allowing an undisturbed view of the ocean surface. However, infrared estimates of sea surface temperature remain of high importance for the computation of evaporation climatology since estimates of sea surface temperature from SSM/I measurements were not possible with sufficient accuracy. Recently, some new methods have been developed that circumvent the bulk formula in the retrieval process by relating the satellite data directly to an existing flux data set, e.g., re-analyses of fields derived from *in situ* data that are assumed to be true. The accuracy of all methods is comparable at a level of $\pm 30\,\mathrm{W\,m^{-2}}$ and $\pm 15\,\mathrm{W\,m^{-2}}$ at weekly and monthly time scales, respectively.

As mentioned in the previous section, there are not sufficient conventional and surface-based radar rainfall estimates over the oceans for the derivation of rainfall fields. A reasonable alternative is the use of satellite remote sensing. Remote sensing of rainfall from satellites started with the statistical analysis of the reflectivity and emissivity of the upper cloud layers at visible and infrared wavelengths, respectively. Because of the small physical correlation between the signal and the rainfall at the surface, this technique leads to acceptable results only if the derived rainfall is integrated over space and time. Owing to the strong variability of rainfall, rainfall climatologies derived using this technique with data from geostationary satellites with their high repetitive cycle build are still the backbone of today's rainfall analyses.

Over water surfaces, passive microwave radiometers deliver a much better information base. The signal at frequencies below 30 GHz is mostly determined by the emission from rain water, which leads to a strong increase of the brightness temperature over the cold background of the sea surface. For higher frequencies, the brightness temperature decreases owing to scattering by ice particles. This information can also be used to estimate the rainfall rate at the surface. Since the launch of the first SSM/I onboard the satellites of the Defense Meteorological Satellite Program (DMSP) in 1987, a continuous time-series of data exists from at least one satellite. Many algorithms have been developed to analyze rainfall using these measurements. On the basis of numerous algorithm intercomparison projects, it has proved almost impossible to find a so-called standard algorithm that performs best for most of the situations investigated. The variability of the cases analyzed showed the quality of some algorithms under certain conditions, but not of one prevailing algorithm. In many cases it was found that the accuracy of the validation data was not sufficient to classify the quality of the satellite algorithms. A prominent data set using combinations of geostationary satellite data, passive microwave data, and rain gauge data is that produced by the Global Precipitation Climatology Project (GPCP).

With the launch of the satellite of the Tropical Rainfall Measuring Mission (TRMM) in 1997, for the first time a space-borne radar can be used to derive the three-dimensional structure of rainfall and the surface rainfall. The combination of instruments onboard the TRMM satellite can be considered as a reference for methods applied to other instruments in space. A calibration of rainfall estimates from other satellites like the SSM/I then delivers an optimal combination of accuracy and temporal/spatial sampling and subsequently consistent rainfall distributions.

Moisture Budget Methodology

The moisture budget methodology tries to compute $E - P$ as a residual from the large-scale atmospheric transports of water vapor using global analyses and re-analysis data sets produced with four-dimensional data assimilation schemes. This technique has a long history, although it usually makes use of rawinsonde data directly. $E - P$ is computed from eqn [2], which is the vertically integrated (from the top of the atmosphere to the surface) equation for the conservation of water vapor.

$$E - P = \frac{\partial W}{\partial t} + \nabla \cdot \frac{1}{g} \int_0^{p_S} q\mathbf{v}\,\mathrm{d}p \qquad [2]$$

W is the total precipitable water, q is the specific humidity, p is pressure (with p_S being the surface pressure), $\mathbf{v}$ is the velocity vector, and g is the standard gravity. Many comparison studies between precipitation fields produced routinely and the GPCP data set found discontinuities in the analyses due to changes in the data assimilation system. Another problem was that rainfall maxima in the analyses were often in the wrong place and too strong. In general, the assimilation systems have been much improved during the last ten years and are more or less consistent with satellite-derived data sets. However, use of this method with different analysis and re-analysis products from the European Center for Medium-range Weather Forecasts (ECMWF), the National Centers for Environmental Prediction (NCEP), and the National Aeronautics and Space Administration (NASA) as input and comparisons to pure model-computed $E - P$ exhibited large differences. The most critical part of this method is the dependence of the moisture budget on the divergence of the velocity field. This is of special importance in the Tropics, where the divergence field is not very well known.

River Inflow

The inflow of fresh water from rivers is not included in most ocean surface fresh water data sets derived from satellites and is also neglected in the residual approach, but it is significant to the global fresh water balance of the ocean. Baumgartner and Reichel estimated from a global hydrological balance calculation that the contribution of river runoff to the balance is as high as 10% of the contribution of precipitation. It might be thought that the impact of the fresh water inflow from the rivers on the buoyancy would be local in comparison to the size of the ocean basins. However, the impact of major rivers like the Amazon or Congo is observable several hundred kilometers away from the mouths of the rivers. Neglecting this contribution would increase the average salinity of the upper Atlantic ocean (the first 50 m) by 1.5 psu after 10 years of integration of a numerical ocean model.

Two major runoff data sets are the Global River Discharge Catalogue published by the International Hydrography Program (IHP) and that issued by the Global Runoff Data Center, and these form the backbone of information on river runoff. IHP data consists of a selection of monthly discharges at 949 stations over six continents (Africa, Asia, North America, South America, Europe and Australia/Oceania), but only 219 stations are listed as corresponding to a direct discharge into an ocean basin. The length of the individual data sets is 19.3 years on average, but varies from 1 year to 100 years. Additionally, a great disparity exists between the different continents, with Europe and North America presenting the longest records. Not included in either data set is the runoff from Arctic and Antarctic regions and the inflow of fresh water from ground water sources.

Analysis of the monthly mean climatology of the direct contribution of rivers to the fresh water flow into the ocean, considering only rivers for which time records longer than two years exist, sums to ~ 0.57 Sv ($1\,\text{Sv} = 10^6\,\text{m}^3\,\text{s}^{-1}$). This estimate is much lower than that of Baumgartner and Reichel, who found 0.73 Sv, which also includes contributions from regions beyond the polar circles, which they estimated from other sources.

Climatology of *E* – *P* Derived from Satellite Data

Figures 2–4 show the seasonally averaged global maps of evaporation, precipitation, and $E - P$ derived from AVHRR and SSM/I data, on a grid with $1^\circ \times 1^\circ$ resolution. The data set was constructed by averaging instantaneous estimates of the components and the flux over 11 years (1987–1998).

Maximum values of evaporation up to $9\,\text{mm}\,\text{d}^{-1}$ are observed over the Kuroshio and Gulf Stream regions in winter (**Figure 2A**) and minimum values below $1\,\text{mm}\,\text{d}^{-1}$ are seen in the eastern equatorial Pacific and Atlantic during all months. Large areas with high evaporation rates of 5–6 $\text{mm}\,\text{d}^{-1}$ are found in the main Trade Wind belts between about 10° and 40° latitude in both the Northern and Southern hemispheres. These high evaporation regions are the major sources of atmospheric water for the global hydrological cycle. Whereas during Northern Hemisphere winter and spring the maximum extent and the highest values are found north of the Equator (**Figures 2A** and **2B**), maximum evaporation is observed in the southern Indian, Atlantic, and Pacific Oceans during Northern Hemisphere summer and fall (**Figures 2C** and **2D**).

The global precipitation pattern is dominated by a strong band of precipitation circling the globe just north of the Equator. This is the region where the northern and southern Hadley circulation cells meet, forming a region of strong surface convergence known as the Intertropical Convergence Zone (ITCZ). Where the maximum precipitation on an annual scale exceeds $6\,\text{mm}\,\text{d}^{-1}$. Another convergence zone in the western tropical Pacific, known as the South Pacific Convergence Zone (SPCZ), is somewhat broader, with precipitation values similar to those in the ITCZ. It extends from the region of Indonesia and the Philippines south-east across the southern Pacific. With the onset of the summer monsoon, the ITCZ, which was earlier located in the southern Indian Ocean, shifts to its northernmost location and merges with the Monsoon trough giving rise to copious rainfall over the Indian subcontinent and the adjacent seas, namely the Arabian Sea and Bay of Bengal (**Figure 3C**).

On an annual scale, the region off the Indonesian islands receives a maximum rainfall of more than $10\,\text{mm}\,\text{d}^{-1}$. Outside the two convergence zones, precipitation rates are significantly lower, with the exception of two regions. Precipitation rates are quite high over the Gulf and Kuroshio Streams, with values as high as in the ITCZ during the period November to March (**Figure 3A**). This feature has not been recognized in rainfall climatologies derived from routine weather observations.

At tropical and subtropical latitudes, between about 15° N and 40° N and between 5° S and 30° S, the eastern parts of the Pacific and the Atlantic ocean are regions where precipitation is below $1\,\text{mm}\,\text{d}^{-1}$. A similar region is found in the Indian Ocean along the east coast of Africa and Saudi Arabia during all months, with a maximum extent over the whole Arabian Sea during winter (**Figure 3A**). In the Southern Hemisphere, west of Australian coast,

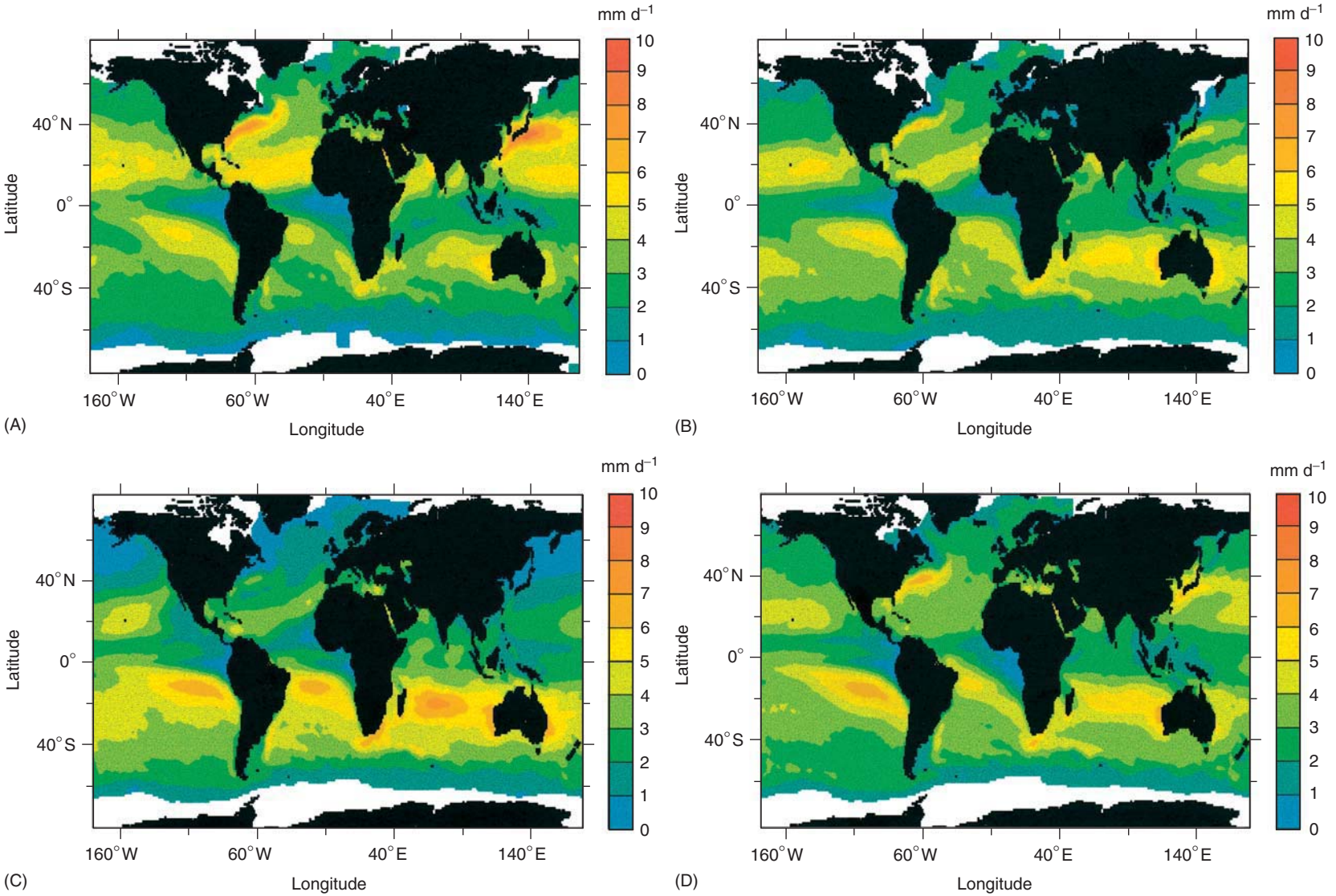

Figure 2 Climatological seasonal averages of evaporation in mm d^{-1} as derived from satellite data: (A) December, January, February; (B) March, April, May; (C) June, July, August; (D) September, October, November.

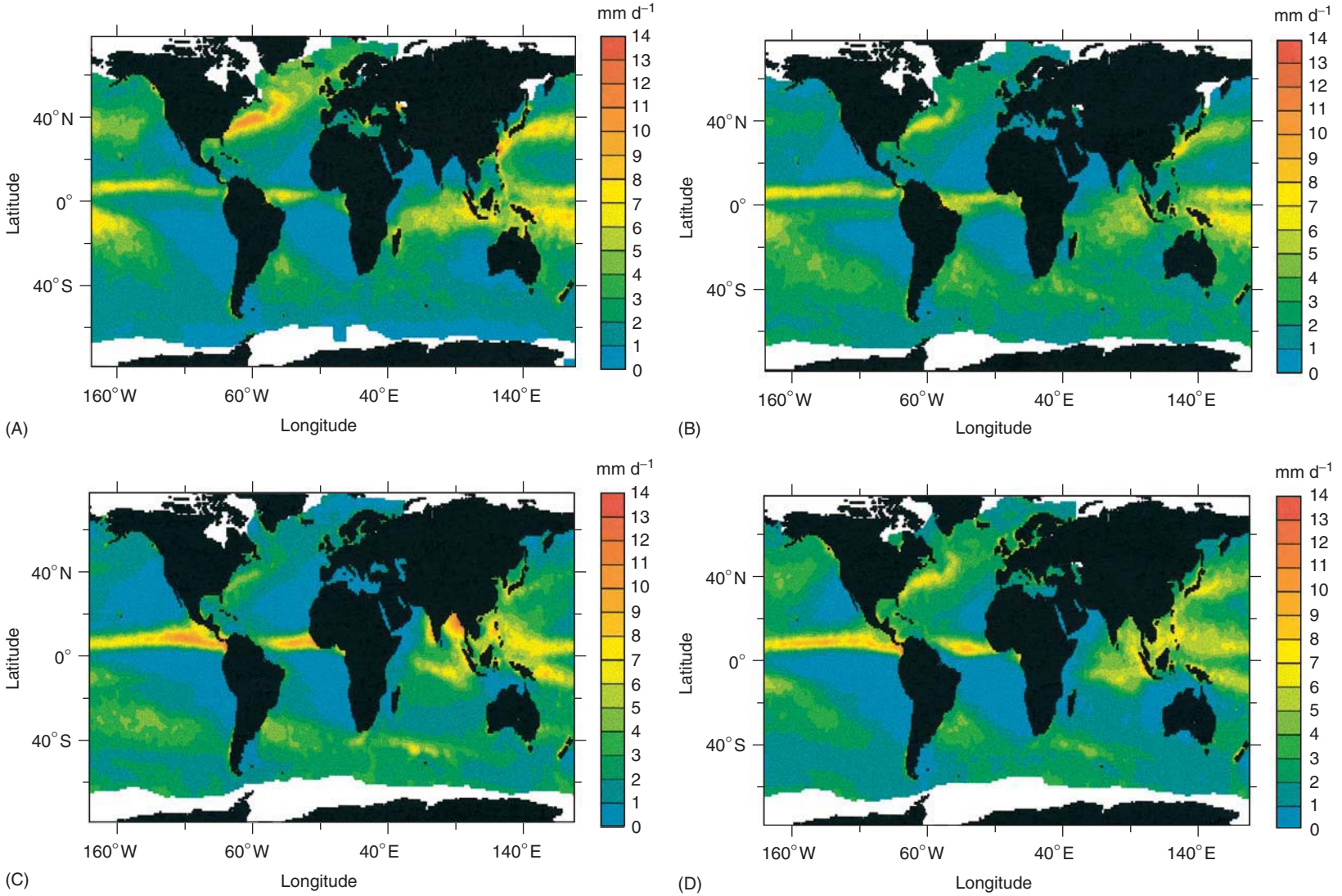

Figure 3 Climatological seasonal averages of rainfall in mm d^{-1} as derived from satellite data: (A) December, January, February; (B) March, April, May; (C) June, July, August; (D) September, October, November.

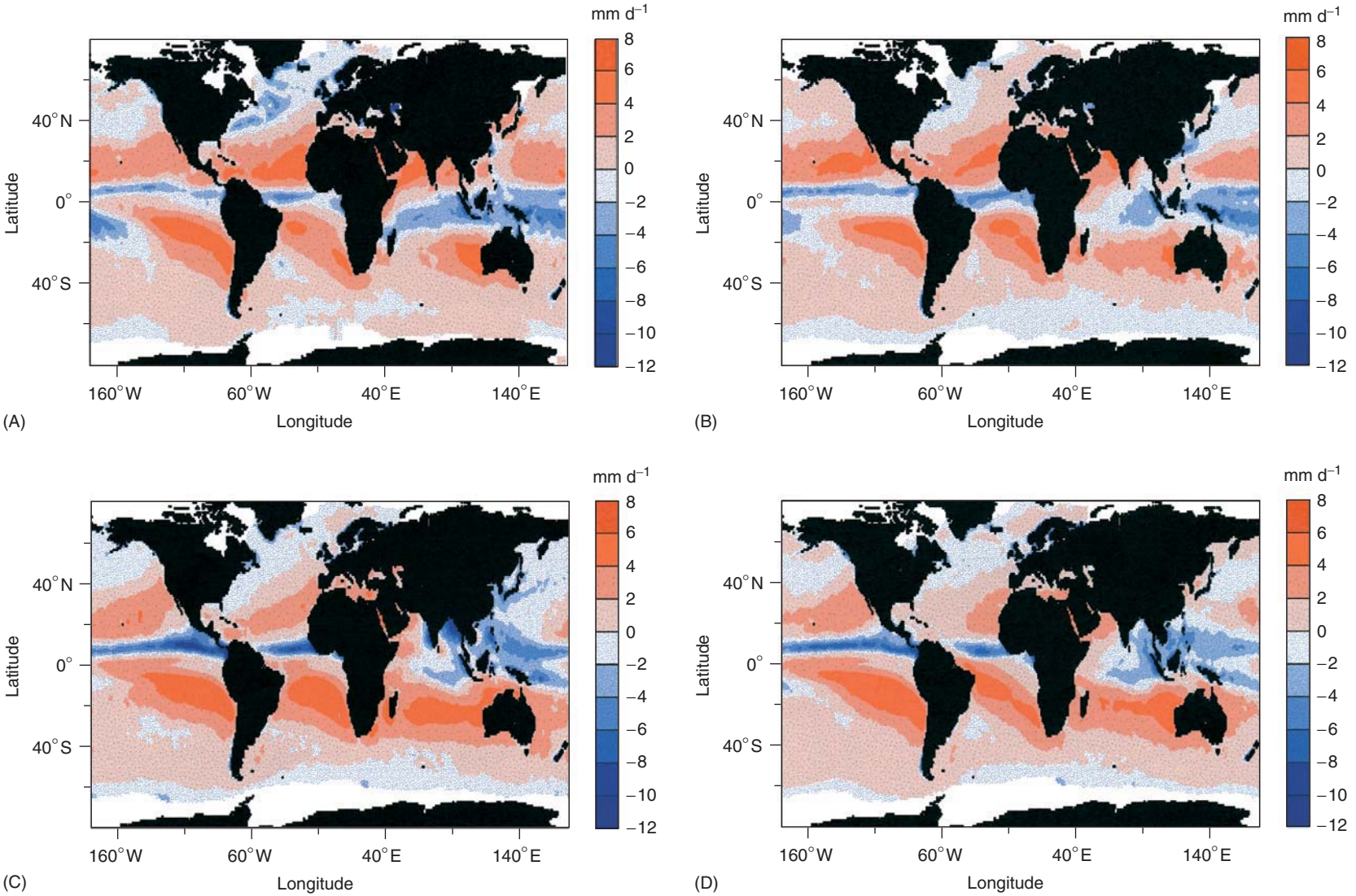

Figure 4 Climatological seasonal averages of $E - P$ in mm d^{-1} as derived from satellite data: (A) December, January, February; (B) March, April, May; (C) June, July, August; (D) September, October, November.

another minimum is observed, which has its maximum extension during the Southern Hemisphere spring (**Figure 3D**).

The patterns of precipitation and evaporation exhibit quite different spatial distributions. Precipitation maxima occur in the global convergence regions, while evaporation maxima occur in regions of high surface humidity gradient and wind speed. On a monthly time scale, values of E exhibit much less spatial structure than fields of P. From this it is clear that the $E - P$ monthly temporal variability is dominated by variations in location and intensity of rainfall and the spatial structure in $E - P$ is also dominated by the P field.

However, on the climatological time scale, fields of $E - P$ consist of signatures of both evaporation and precipitation fields. The ITCZ and SPCZ appear prominently as regions of fresh water supply to the ocean. In these regions the fresh water flux from atmosphere to ocean is generally larger than $4\,\mathrm{mm\,d^{-1}}$. With the exception of the SPCZ, precipitation decreases rapidly with latitude to the north and to the south of the ITCZ, while evaporation remains strong or even increases, causing positive values of the fresh water flux.

The strongest gradients in the fresh water flux fields occur in the boundary regions between the negative values of $4\,\mathrm{mm\,d^{-1}}$ within the ITCZ and the strong positive flux regions to the north and south, with values up to $6\,\mathrm{mm\,d^{-1}}$. Poleward from the evaporation regions, the fresh water flux is relatively small. The evaporation fields generally decrease toward the poles primarily as a result of the decrease in the humidity difference, except during wintry arctic cold air outbreaks which often lead to very high evaporation rates and therefore to positive fresh water fluxes. Although evaporation is quite high, large negative values of $E - P$ can be found in the Gulf Stream and Kuroshio regions, below $-4\,\mathrm{mm\,d^{-1}}$ during the winter owing to high precipitation, while in all other months evaporation almost balances precipitation.

An analysis of the fresh water flux on a seasonal scale (**Figures 4A–D**) reveals that the eastern parts of the Arabian Sea, the Bay of Bengal, and the South China Sea all have negative values of fresh water flux during summer (**Figure 4C**) and autumn (**Figure 4D**). Further, on an annual scale, it can be seen that the eastern equatorial Indian Ocean, the Bay of Bengal, and the Kuroshio and the Gulf Stream regions all exhibit negative fluxes. The regions of positive flux are over the north-west Arabian Sea and the southern Indian Ocean south of 20° S. Also, the North Atlantic and the South Atlantic exhibit positive fluxes on both sides of the ITCZ.

Table 1 Global climatological averages for E, P, and $E - P$ (in $\mathrm{mm\,d^{-1}}$) over oceans, from different studies

Source	*E*	*P*	*E* − *P*
Baumgartner and Reichel (1975)	1177	1066	111
Chahine (1992)	1202	1088	114
ECHAM4[a] (Todini and Dümenil, 1999)	1246	1147	99
ECMWF[b]+GPCP[c] rain (Oki, 1999)	1194	1083	111
HOAPS[d] (Grassl *et al.*, 2000)	1086	908	178

[a]ECHAM4: Cimate model of the Max-Planck Institute for Meteorology, Hamburg.
[b]ECMWF: European Centre for Medium-range Weather Forecasts.
[c]GPCP: Global Precipitation Climatology Project.
[d]HOAPS: Hamburg Ocean Atmosphere Parameters and Fluxes from Satellite Data.

Discussion and Conclusion

Table 1 shows how existing estimates of the fresh water flux and its components differ from some examples of estimates from different sources found in the literature. Whereas the older estimates from observations are comparable to the results from General Circulation Models, the satellite estimates differ considerably from all of them. However, today there is no agreed true value for $E - P$. Current results of global analyses seem not to be very reliable, but centers like ECMWF are improving the assimilation of rainfall estimates from satellite data, and these will be operational in a few years. Satellite data sets have great potential to be improved in the future by using sophisticated methods of intercalibration between different satellites. In the case of basic state variables U, Q_a, and T_S, improvements are expected from intercomparison of the satellite estimates with high-quality surface-based measurements.

See also

Aerosols: Climatology of Tropospheric Aerosols. **Air–Sea Interaction:** Momentum, Heat and Vapor Fluxes; Sea Surface Temperature. **Clouds:** Climatology. **Data Analysis:** Time Series Analysis. **Humidity Variables**. **Satellite Remote Sensing:** Precipitation. **Turbulent Diffusion**. **Weather Prediction:** Data Assimilation.

Further Reading

Baumgartner A and Reichel E (1975) *The World Water Balance*. Muenchen Wien: R. Oldenbourg Verlag.

Chanine MT (1992) The hydrological cycle and its influence on climate. *Nature* 359: 373–380.

Grassl H, Jost V, Schulz J, *et al*. (2000) *A Climatological Atlas of Satellite-derived Air–Sea Interaction Parameters over the Worlds Ocean*, Max-Planck Report No. 312. Hamburg: Max-Planck Institute for Meteorology. URL: http://www.mpimet.mpg.de/Depts/Physik/HOAPS

Hartmann DL (1994) *Global Physical Climatology*. San Diego: Academic Press.

Josey S, Kent EC and Taylor PK (1999) New insights into the ocean heat budget closure problem from analysis of the SOC air–sea flux climatology. *Journal of Climate* 12: 2856–2880.

Oki T (1999) The global water cycle. In: Browning KA and Gurney RJ (eds) *Global Energy and Water Cycles*, pp. 10–27. Cambridge: Cambridge University Press.

Taylor PK (ed.) (2000) *Intercomparison and validation of ocean–atmosphere energy flux fields*. Final report of the Joint WCRP/SCOR Working Group on Air–Sea fluxes, WCRP-112, WMO/TD No. 1036. URL: http://www.soc.soton.ac.uk/JRD/MET/WGASF

Todini E and Dümenil L (1999) Estimating large-scale runoff. In: Browning KA and Gurney RJ (eds) *Global Energy and Water Cycles*, pp. 265–277. Cambridge: Cambridge University Press.

Trenberth KE and Guillemot CJ (1999) Estimating evaporation-minus-precipitation as a residual of the atmospheric water budget. In: Browning KA and Gurney RJ (eds) *Global Energy and Water Cycles*, pp. 236–246. Cambridge: Cambridge University Press.

Gas Exchange

P D Nightingale, Plymouth Marine Laboratory, Plymouth, UK

Introduction

The air–sea interface acts as the conduit for the transfer of gases such as oxygen, dimethyl sulfide, carbon monoxide, carbon dioxide, and methyl iodide between the oceans and atmosphere. The air–sea interface is therefore of fundamental importance in studies of marine productivity, biogeochemical cycles, atmospheric chemistry, climate, and human health. For example, about 30% of the world's population is at risk of iodine deficiency disorders that impair mental development. The main supply of iodine to land is the transfer of volatile iodine compounds produced in the oceans to the atmosphere via the air–sea interface. A further example is that the oceans take up about 30% of the anthropogenic CO_2 annually emitted to the atmosphere and represent the long-term sink for most of the predicted future emissions of anthropogenic CO_2.

It has proved to be extremely difficult to measure air–sea gas fluxes *in situ*. As a result, they have been calculated from the product of the concentration difference between the two phases and a kinetic (or rate) term known as the gas transfer coefficient (k). The gas transfer coefficient is also known as the transfer velocity as it has dimensions of length per unit time. As most gases of interest are produced and/or destroyed within the ocean or atmosphere, there is considerable spatial and temporal variability in concentration fields. Large international research programs have attempted to quantify this variability and to understand gas production and removal mechanisms, with the aim of predicting concentration fields by using oceanic/atmospheric models.

Rather less progress has been made in understanding the basic mechanisms behind air–sea gas transfer, although the two most important variables are molecular diffusivity and the degree of turbulence close to the air–water interface. One of the main parameters linked to turbulence is wind speed, although observations from laboratory studies suggest that other variables such as surfactants, breaking waves, and bubbles also influence k. Although models predict that k should rise with increasing wind speed (or more correctly friction velocity), the dominant mechanism is not agreed upon. A major problem is a dearth of knowledge concerning the sea surface microlayer (usually defined as the top 1 mm of the sea) and its properties.

Given the lack of a comprehensive understanding of the processes controlling gas exchange, various ingenious techniques have been developed to try to measure k *in situ* in order to develop and test parameterizations based on easily measurable and readily available environmental variables such as wind speed. An improvement on wind speed-based parameterizations is dependent on a better understanding of the processes controlling air–sea exchange and on new techniques to measure k over short time scales.

The Two-Film Model of Gas Exchange

The simplest model of air–sea gas transfer is the two-film model illustrated in **Figure 1**. Although physically unrealistic, it is useful in visualizing how gas transfer between the two interfaces may occur. The model assumes that the main bodies of air and water are well mixed and that transfer through the two thin films is by